# Landslide hazard zoning: from the view point of landscape development

Disaster Prevention Research Institute, Kyoto University ○Ching-Ying TSOU, Masahiro CHIGIRA, Yuki MATSUSHI,
Department of Soil and Water Conservation, National Chung Hsing University Su-Chin CHEN

## 1. Introduction

Evaluating an aerial hazard level of landslide is very important to mitigate the landslide disaster and there have been several approaches for it: Physical modeling, statistical modeling, geological and geomorphological characterization, and geomorphological classification. The first three approaches are to pinpoint potential sites and the last one is to classify hazard potential over wider areas, which, however, comparatively little research has been conducted. We propose to classify the hazard level based on geomorphological classification from the view point of landscape development according to the landslide sits in relation to convex slope breaks.

## 2. Study area

The study area in the upstream section of the Dahan River catchment in northern Taiwan covers 503.8 km$^2$. The Dahan River cuts the Eocene and Miocene sedimentary rocks and slate and flows northward in mountains with summit elevations of 1200 to 3529 m a.s.l.. Episodic landslide events have occurred during rainstorms, and the precipitation from Typhoon Aere in 2004 caused the most severe damage to the catchment in recent decades (Fig. 1). On both sides of the Dahan River, Tsou et al. (2014) have observed that hillslopes contain three subsidiary convex slope breaks and have traced the distribution of these slope breaks (Fig. 2). The slope breaks at higher elevations (hereinafter referred to as "$B_H$") are as much as around 600 m above the current riverbed at the rims of widespread paleosurface remnants. Additional two slope breaks were observed at around 300 and 100 m above the current riverbed (hereinafter referred to as "$B_M$" and "$B_L$", respectively) on the lower slopes of three-story V-shaped inner gorges. The paleosurface remnants have an average slope angle of 31.9°, which are incised by inner gorges with average slope angles of 35.6°, 37.7°, and 39.8°. The inner gorges are formed over time associating with slope movement and the long-term river incision.

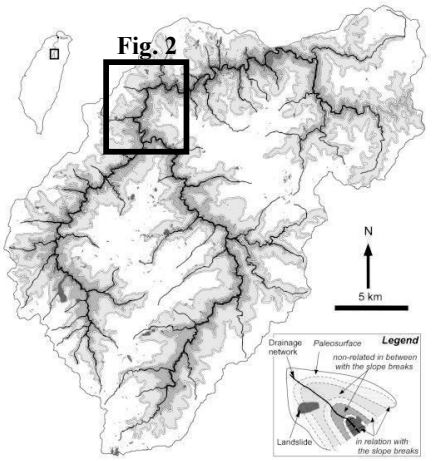


Fig. 1. Distribution of landslide scars and slope beaks.

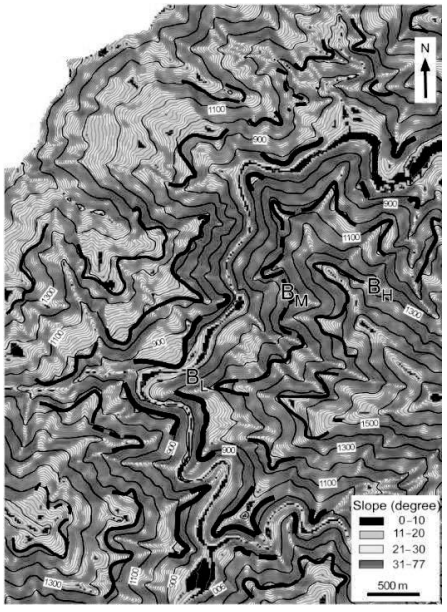


Fig. 2. An example of the distribution of slope breaks (lines).

## 3. Landslide characteristics and their distributions

Landslide scars were delineated using orthorectified aerial photos (with a resolution of 0.5 m) taken after the 2004 Typhoon Aere by Soil and Water Conservation Bureau of Taiwan (Fig. 1). In total, 2045 landslide scars were mapped with landslide areas that span four orders of magnitude from $5.7 \times 10^{-5}$ to $6.5 \times 10^{-1}$ km$^2$. Cumulative area-frequency analysis shows that landslides having areas of less than $1.7 \times 10^{-3}$ km$^2$ accounted for 50 % of the total landslide number but for only 9% of the total landslide area (9.6 km$^2$). The analysis also demonstrated that landslides of larger than $1.0 \times 10^{-1}$ km$^2$ value account for 0.2% of the total landslide number and 11% of the total landslide area. The results suggest the importance of the smaller and larger landslides. To differentiate the potential locations of the larger and smaller landslides, analysis of the geographic distribution of landslide scars were conducted by examining their source areas whether or not involved with the slope break buffering zones. A horizontal distance of 40 m from a specific slope breaks line was set to account for the mapping errors associated with the landslides and break lines themselves. Consequently, landslide

scar inventory was subdivided into six sub-categories: along $B_H$ ($N = 262$), $B_M$ ($N = 430$), $B_L$ ($N = 447$), between $B_H$ and $B_M$ ($N = 347$), between $B_M$ and $B_L$ ($N = 188$), and on the paleosurface ($N = 371$).

Figure 3 shows the landslide density of each of the sub-categories, indicating landslides occurred much more frequently on the slope breaks with densities of 7.2, 16.6, and 20.1 $km^{-2}$ for landslides on the slope breaks, $B_H$, $B_M$, and $B_L$, respectively. In contrast, landslides are relatively infrequent away from the slope breaks with lower densities of 1.7, 2.5, and 3.2 $km^{-2}$ on the paleosurface, between $B_H$ and $B_M$, and between $B_M$ and $B_L$. The results suggest that landslide scars are concentrated along the slope breaks.

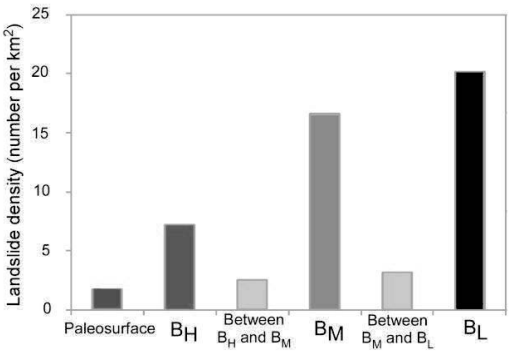

Fig. 3 Landslide density along and away from the slope breaks.

Probability density distribution of landslide area is useful to assess landslide magnitude and frequency and methods used to calculate the distribution follow the approach explained in detail by Malamud et al. (2004). Figure 4 shows that medium–large landslides (>$6.0 \times 10^{-4}$ $km^2$) are more common on slopes along $B_H$ and $B_M$ and numerous small landslide scars are evident around $B_M$. On the other hand, small landslides (<$5.0 \times 10^{-4}$ $km^2$) are most abundant on slopes along $B_L$. The inverse power law scaling exponents (linear in log-log axes portion of the distribution) for landslides along $B_H$, $B_M$, and $B_L$, were 0.7, 0.8, and 1.2, respectively. These estimates suggest that the subset of data may be biased towards larger landslides for landslides along $B_H$ and $B_M$.

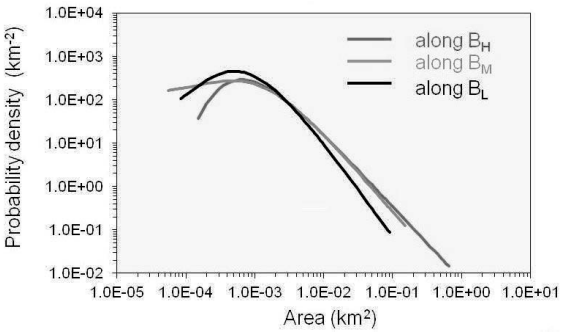

Fig. 4 Probability density distributions of landslide areas along the slope breaks.

## 4. Landslide volume

Although there is no comprehensive data set for estimation of landslide volume ($V$) covering the study area as yet, there is currently a major empirical relationship. In the downstream section within our study area, Chen et al. (2010) derive the $V = 0.015A^{1.606}$ from 560 landslides with areas between $10^{-5}$ $km^2$ and $10^{-1}$ $km^2$. This empirical relationship may be of use for shallow and deep-seated landslides. According to the relationship, the cumulative volume of landslides along $B_H$ was 47.5 $km^3$, along $B_M$ 17.6 $km^3$, and along $B_L$ 7.1 $km^3$, accounting for 56%, 21%, and 8% of the total landslide volume (84.8 $km^3$) respectively.

## 5. Conclusion

Our analyses reveal that larger landslides tend to occur along higher slope breaks, while small landslides occur along all three slope breaks, but with higher frequencies along the lower slope breaks. These probably represent constraints on landslide size due to geomorphic process, attributing to the destabilization of slopes due to undercutting by the river incision that formed the slope breaks. The coupling of channels and hillslopes over long periods of time creates favorable condition for landslide generation, as the relative height of the slope break influences the maximum potential size, while the threshold hillslope gradient controls the occurrence of the failures. The results indicate that landslide sites can be predicted from the view point of landscape development by understanding the distribution of slope breaks, which can be used for the hazard level zoning of landslide.

*Finally, it is noted that this report is mainly based on Tsou et al. (2014), from which more detailed information on landscape development of the study area could be obtained.*

## References

Chen, S.-C., Weng, K.-L., Wu, C.-H., 2010. The characteristics of landslides and landsldie size in Yu-Fong river watershed. Journal of Chinese Soil and Water Conservation, 41(3), 217-229. (in Chinese, with English Abstract).

Malamud, B.D., Turcotte, D.L., Guzzetti, F., Reichenbach, P., 2004. Landslide inventories and their statistical properties. Earth Surface Processes and Landforms, 29(6), 687–711.

Tsou, C.-Y., Chigira, M., Matsushi, Y., Chen, S.-C., 2014. Fluvial incision history that controlled the distribution of landslides in the Central Range of Taiwan. submitted to Geomorphology.